A Simple Approach to MXene Micropatterning from Molecularly Driven Assembly

Linh Chi T. Cao, Chao-An Jong,* Shu-Han Hsu,* and Shih-Feng Tseng*

Cite This: *ACS Omega* 2021, 6, 35866−35875

Read Online

ACCESS | Metrics & More | Article Recommendations | SI Supporting Information

ABSTRACT: Here, a micropatterning strategy is demonstrated to achieve stable and selective MXene adsorption through the molecularly driven assembly. MXene flakes were assembled by strong interaction with a silicon substrate, which was functionalized by microcontact printing (μCP) to create an active surface. A clear micropattern was observed by scanning electron microscopy showing uniform coverage of MXene flakes. Atomic force microscopy revealed a pattern thickness of around 50 nm, much thinner than the patterns obtained by direct μCP. The obtained micropattern presents good stability against rinsing and sonication. X-ray photoelectron spectroscopy shows that this stability can be attributed to strong covalent bonding between MXene and active molecules on a silicon substrate. The sheet resistance of the as-formed MXene layer was measured at around 154.67 ($\Omega/\square$), which is lower than those of other published techniques with a similar thickness of around 50 nm. This method can achieve a well-defined MXene pattern around the sub-100 μm scale without requiring prior MXene surface modification. Therefore, MXene can retain its intrinsic surface property, allowing further molecule adsorption as a sensing platform. Moreover, this patterning technique does not require complicated control of ink preparation and offers possible application on a substrate of any geometry with few layers of thickness.
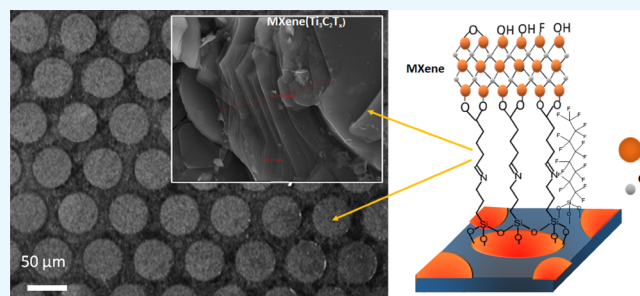
1. INTRODUCTION

MXenes, a new group of 2D materials, combine excellent dispersion quality and hydrophilic surfaces with good metallic conductivity. Many explorations show their possible applications for energy storage,[1,2] electromagnetic shielding,[3] nanocomposite fabrication,[4,5] water purification, and different kinds of sensors with such fascinating properties.[6−10] From responsive mechanical stretching,[11] heavy-metal monitoring,[12,13] and biomolecule probing[14] to various-gas detection,[15] MXene materials offer many possibilities with improved performance.

Today, MXene materials are still synthesized in a solution-based process. Recent developments focus on immobilizing and patterning those solution-processed 2D materials in a precisely defined area to fabricate sensing devices. Zhang et al. reviewed current MXene printing and patterned coating for device applications.[16] They made a detailed discussion with up-to-date MXene patterning demonstration including inkjet printing, screen printing, 3D printing, ink writing, patterned coating, and transfer printing. It is worth noting that these printing technologies required proper preparation of the MXene ink. Chemical stability, ink storage, and rheological properties need to be carefully optimized for an individual printing technology to reproduce the printing process and the quality of printed patterns. However, the rheological requirements for different printing/coating methods vary significantly from viscous paste for 3D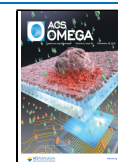 printing and screen printing to a low-concentration solution dispersion for inkjet printing. Moreover, such ink-related printing technologies can easily obtain micrometer thickness, while thickness reduction will need careful process optimization, especially around a few hundred nanometers.

Theoretical studies predict that the conductive property of MXenes can vary from metallic such as $Ti_3C_2T_x$ to semiconductor-like on certain Mo- and V-based MXenes.[17−19] Today, the understanding that controls MXene conductivity is strongly related to its surface terminal group, introduced during MXene synthesis.[18,20] However, an additional mechanism that can affect MXene conductivity is intercalation, especially for multilayer MXene samples. That is to say that for any multilayer MXene sample, the measured electronic conductivity is closely related to the intercalation, termination, and $M_{n+1}X_n$ chemistry. This convolution of effects complicates experimental interpretation, especially limiting the consistency as a sensing device. Therefore, obtaining an MXene pattern with a few layers/monolayer structures is trivial for under-

standing its electronic property without altering its pristine surface chemistry, especially for electronic sensing device application. Moreover, the lower the electrical resistivity, the higher the electrical conductivity of the sensing material layer. In addition, the electrical resistivity depends on sheet resistance and the thickness of the material layer. Hence, to obtain a high conductivity of the MXene layer, it is important to form a thin MXene film with a low sheet resistance.

Transfer printing is one of the techniques that has been employed for layered MXene delivered from the MXene source onto the desired substrate using a soft polymeric stamp.[14] With polymeric stamps (commonly using polydimethylsiloxane, PDMS), transferring target micro-objects was successfully demonstrated through conformal contact between the target substrate and the stamp. This is the so-called "microcontact printing" (μCP).[21] Patterning is achieved simultaneously with a prepatterned stamp to define the active area for selective material adsorption. The interfacial bonding strength between the stamp surface and target solution should be weaker than that of the solution and the targeted substrate surface to fulfill the transferring purpose. Thus, the target solution can be easily released from the stamp. This transfer printing, or named the soft lithography technique, was used to create monolayer patterns with consistent quality for quite a range of studies.[22,23] This microcontact printing technique was used previously to transfer nanoparticles, such as gold and TiO_2 nanoparticles.[24,25] However, limited research was demonstrated for transferring bigger objects from a few hundred nanometers to submicrometers for wider-scale patterning, such as nanotubes, nanosheets, and even layered 2D material flakes.[26,27] Such object transfer requires particle size considerations, chemical modification over a stamp prior to pickup, or special inking solution preparation to achieve qualitative and large-scale patterning.

Some publications revealed patterning of 2D materials onto a silicon substrate. For example, a study by Xiao et al. developed micropatterning of graphene oxide nanosheets directly to achieve size-adjustable patterns on substrates in a large area via hydrogen bonds between GO flakes and the hydroxyl-terminated surface.[28] Another study was also published using PDMS stamps to directly transfer MXene onto a glass substrate, modified by amine-containing molecules to obtain an ultrathin layer of MXene.[14] These approaches successfully immobilized 2D materials but limited layer stability, pattern qualities, and thickness reduction.

In this study, taking advantage of the natural property of the MXene ($Ti_3C_2T_x$) surface that has a surface functional group ($T_x = -O$, $-F$, or $-OH$) and a highly negative charge, the chemical bonding or electrostatic interaction behaviors between the surface-active functional groups and MXene are evaluated. The μCP and backfilling processes create the chemical patterns on a silicon wafer with different functional groups. Moreover, these patterns will serve as a template to guide MXene adsorption and be visualized by scanning electron microscopy. Herein, we report a new strategy to obtain MXene flakes' micropatterns without altering their pristine property with stable and area-controlled MXene adsorption with few nanometers of thickness and a low resistivity of the obtained MXene layer.

2. EXPERIMENTAL SECTION

2.1. Materials. Titanium aluminum carbide (Ti_3AlC_2; 98.2%, Luoyang Tongrun Info Technology Co., China),

lithium fluoride (LiF; 97%, Acros Organics), and hydrochloric acid (HCl; 37%, Carlo Erba) were used as etchants for the MXene ($Ti_3C_2T_x$) synthesis process. A silicon wafer (n-type, 6 inches, Biotin Crystal Co., Ltd., China) was used as a substrate for MXene patterning and used to fabricate the masters to create PDMS stamps. A Sylgard 184 silicone elastomer kit (PDMS) (Dow Chemicals) with a polymeric base and a curing agent was utilized. (3-Aminopropyl)-triethoxysilane (APTES; 98%, Sigma-Aldrich) and $1H,1H,2H,2H$-perfluorooctyltriethoxysilane (POTS; 98%, Sigma-Aldrich) were used to form self-assembled monolayers with silicon substrates. Glutaraldehyde (GA) with 25% in H_2O (Sigma-Aldrich) was used as a cross-linking reagent between APTES and the MXene material. Ethanol (C_2H_5OH; 99.9%, Duksan, Korea) was used as a solvent to dilute APTES. Sulfuric acid (H_2SO_4; 96%, Carlo Erba) and hydrogen peroxide (H_2O_2; 35%, ChemSupply) were used to create piranha solution for silicon surface activation.

2.2. Synthesis of $Ti_3C_2T_x$. $Ti_3C_2T_x$ was produced by selective etching of aluminum layers from their parent Ti_3AlC_2 phases. The etching process by lithium fluoride (LiF) in hydrochloric acid (HCl), known as the "minimally intensive layer delamination (MILD) method", was modified with an extra etching cycle to have better delamination.[29] The molar ratio of LiF to Ti_3AlC_2 as 7.5:1 was used in 6 M HCl as indicated in the MILD method. The first etching process started with mixing for 3 h at 45 °C and subsequent cooling down to room temperature for 21 h under continuous stirring (500 rpm). The products were washed several times with centrifugation (5 min/cycle) using deionized water (DI water) until the final pH value was about 5−6. The obtained solution was slowly separated into two parts, which were the supernatant dispersed at the top of the solution and the sediment settled at the bottom of the centrifuge tube. After the first etching process, the sediment was collected and dried in a vacuum oven at 70 ° C for 24 h. This sediment was dispersed in a freshly prepared LiF−HCl solution for another run of the etching process as described above. However, no heating was applied under stirring at room temperature for 24 h. Finally, the mixture was subsequently alkalized with 1 M NaOH solution for 2 h at room temperature. Then, the product mixture was washed and separated into the supernatant and the sediment after solution neutralization.

2.3. Stamp Preparation. Two types of polydimethylsiloxane (PDMS) stamps were fabricated using a replica-molding technique from two kinds of negative silicon masters. Two different trench depths were fabricated with a 17.6 μm depth for direct MXene printing with 100 μm dots and a 1 μm depth for APTES printing with 50 μm dots. The PDMS stamps were treated with O_2 plasma (100 W) for 1 min and stored in DI water before use.

2.4. Molecularly Driven Patterning Procedures. The 0.1% APTES solution was diluted in absolute ethanol, dropped onto a plasma-treated stamp, and dried with N_2 gas for 1−2 min. The APTES-coated stamp was printed lightly on a silicon wafer (1 cm × 1 cm) for 5 min. After stamp removal, silicon was rinsed with ethanol intensively to remove the physical adsorption of APTES molecules. The silicon sample with APTES patterns was obtained (APTES SAM). After that, the silicon sample was put inside a desiccator with $1H,1H,2H,2H$-perfluorooctyltriethoxysilane (POTS) under vacuum conditions for 24 h self-assembly of POTS onto a nonpatterned area of the silicon surface. The 5% glutaraldehyde solution in DI water was prepared, and the silicon sample with APTES SAM
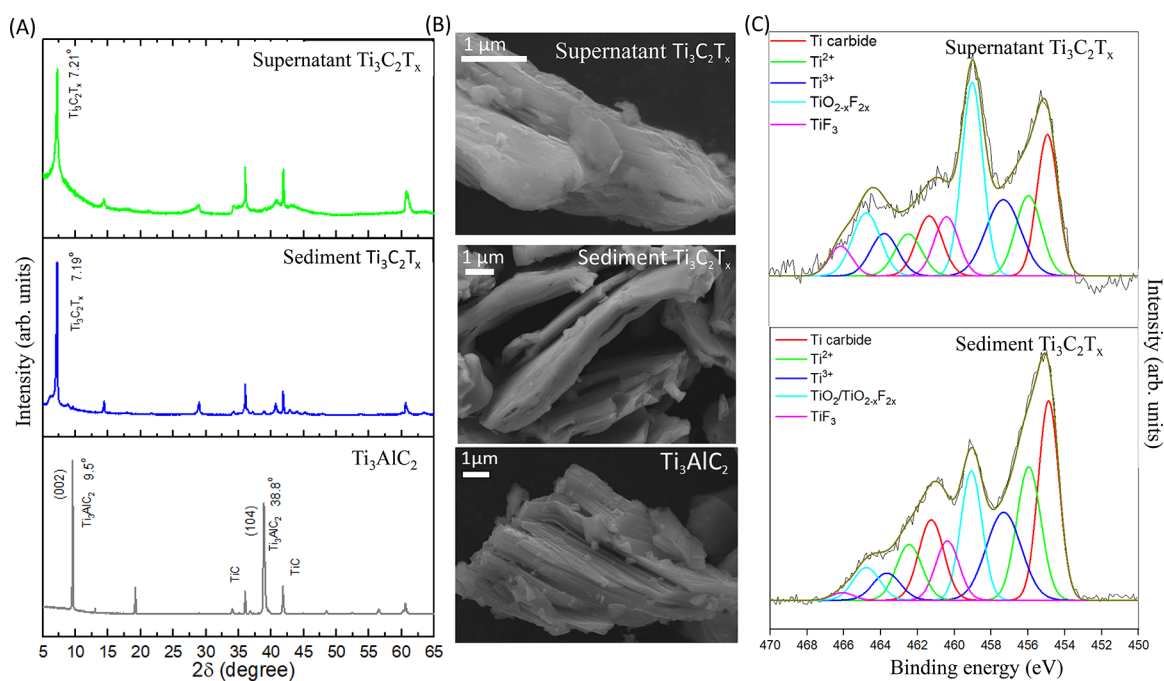
Figure 1. Characterization of bulk MXene. The as-synthesized MXene is separated into a supernatant and a sediment. (A) XRD patterns of the transition from Ti_3AlC_2 to $Ti_3C_2T_x$ as the (002) shifts to lower diffraction angles. (B) SEM images of the multilayer structured MXene. (C) High-resolution XPS spectra of Ti 2p.

patterns was immersed for 24 h and rinsed with DI water. Then, it was followed by incubation in 25 mg/mL MXene solution (sediment $Ti_3C_2T_x$) with HCl as a catalyst (final pH ~ 3−4) for 24 h to allow chemical selective adsorption of MXene. After MXene immobilization, the silicon sample with MXene patterns was rinsed with DI water followed by soft-mode sonication for 5 min to remove the excess MXene that adsorbed onto silicon.

2.5. Direct Printing Process. Silicon substrates were hydrolyzed in piranha solution (H_2SO_4:H_2O_2 = 3:1) at room temperature for 15 min followed by repeated rinsing and stored in DI water for the following stamping procedure. Ten microliters of 25 mg/mL $Ti_3C_2T_x$ solution was applied to cover stamps uniformly and dried under nitrogen gas. The inking stamps were then gently applied onto a silicon wafer (1 cm × 1 cm) for 5 min with 0 and 35 g weights. Following stamp removal, silicon samples were rinsed with DI water and sonicated for 5 min to remove excess materials. The 25 mg/mL $Ti_3C_2T_x$ solution was prepared by dispersing MXene powder in DI water by sonication for 5 min.

2.6. Chemical and Morphological Characterization. A scanning electron microscope (SEM) with a tungsten-heated cathode (VEGA3, TESCAN, Czech Republic) was used for EDX mapping. Moreover, a field-emission scanning electron microscope (FESEM) (JEOL JSM7800F, Japan) with a higher magnification was used for the morphological observation due to its good image quality. X-ray diffraction (XRD) (Bruker AXS model D8 Advance, Germany) was used to identify the crystal structure and compound types of as-synthesized Ti_3AlC_2 phases and MXene products. The condition was measured at 2θ angles between 4 and 80° with Cu Kα irradiation (λ = 1.5406 Å) at 40 kV at room temperature. The detector was a LYNXEYE XE-T. The increments were 0.02 degree/step and 0.2 s/step. X-ray photoelectron spectra (XPS) were obtained on a Thermo Fisher Scientific theta probe,

which was equipped with a monochromatic Al Kα X-ray source and operated at 1486.6 eV. Spectra were referenced to the main C 1s peak set at 284.0 eV. The X-ray beam size was varied from 15 to 400 μm. The data were collected from a surface area of 100 μm × 300 μm with a pass energy of 224 eV, with step energy values of 0.8 eV for survey scans and 0.4 eV for high-resolution scans. For quantitative analysis, the sensitivity factors used to correct the number of counts under each peak were as follows: C 1s, 1.00; N 1s, 1.59; Li 1s, 0.061; Al 2p, 0.56; Cl 2p, 2.741; Ti 2p, 6.471; O 1s, 2.881; F 1s, 4.118. The measurement was collected after 25 cycles of scanning. Water contact angles (WCA) were measured by a Dino-Lite digital microscope system, focusing on a magnification of around 20−25× with 10 μL of DI water dropping on surface samples. The angles were identified by DinoCapture 2.0 analysis software. In addition, an atomic force microscope (AFM) (Veeco Dimension 5000) in tapping mode was used to analyze the morphologies and dimensions of the MXene patterns with a scan rate of 0.8 Hz and 512 lines/sample. The sheet resistance was measured by using a four-point probe (JANDEL model MR3) with a 1 mm distance between the probes. The measurement was repeated at least 5−10 times at different positions of each film. The average values were presented.

3. RESULTS AND DISCUSSION

To improve the adsorption performance of MXene, alkali solution (NaOH) was added to increase more hydroxyl −O/−OH functional groups on the surface.[6] Figure 1A displays the detected XRD pattern showing the transformation from Ti_3AlC_2 (MAX) to $Ti_3C_2T_x$ (MXene). The identical peak for $Ti_3C_2T_x$ formation, such as the (002) peak of the MAX phase at 9.5°, broadened and shifted to lower angles at ~7.2°, indicating the that Al atom was etched, exfoliated, and replaced by surface moieties (−O, −F, and −OH).
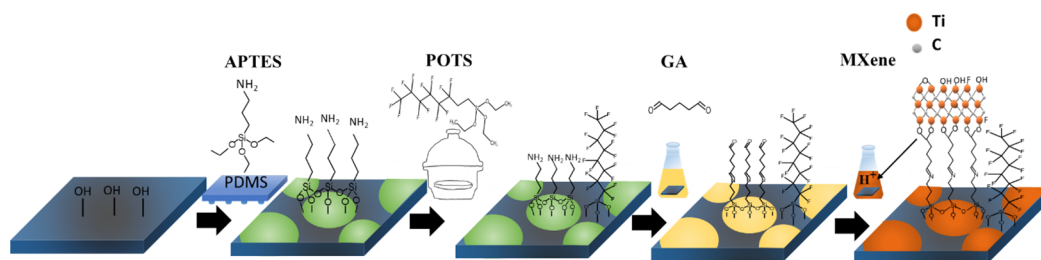
Figure 2. Schematic of the stepwise process to obtain micropatterns of MXene via chemical bonding formation.
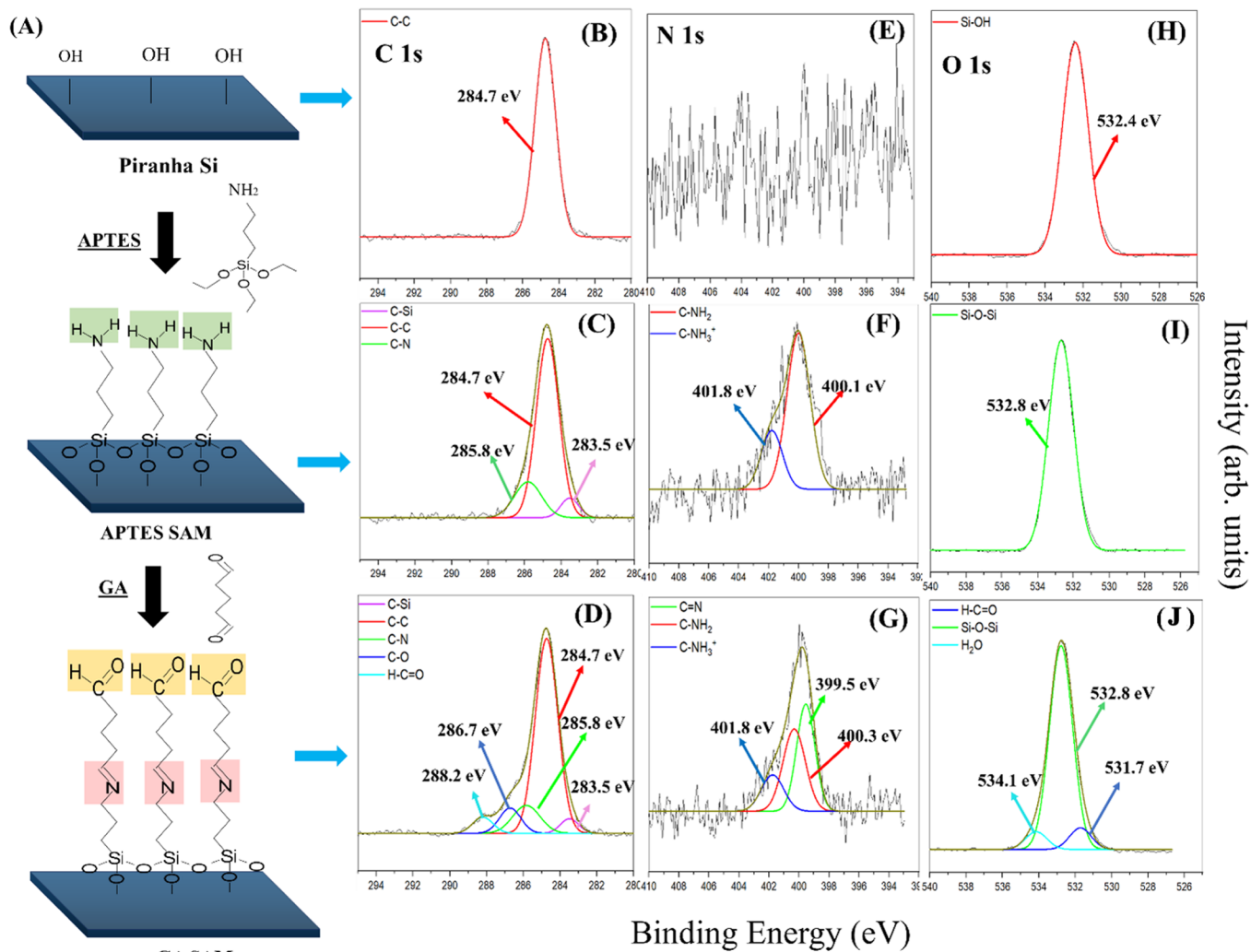

Figure 3. (A) Schematic illustration of the procedure for the monolayer formations onto a silicon substrate. Peak fitting of XPS C 1s (B−D), N 1s (E−G), and O 1s (H−J) spectra of functional modification on the silicon substrate after piranha solution, APTES SAM, and GA SAM formations, respectively.

XPS is currently an essential tool to understand the surface chemistry of MXenes, and several recent papers have reported on the spectral decomposition of the different peaks associated with MXenes.[30,31] Insights into the surface chemical structure of synthesized MXene are revealed by XPS characterization (Figure 1C). In the survey region (0−1200 eV), the signals from elements C, Ti, O, and F could be detected (see Supporting Information Figure S1). The Ti 2p spectrum contains five doublets at the Ti $2p_{3/2}$ and Ti $2p_{1/2}$ regions. The Ti^{4+} bond at 459.1 eV belongs to TiO_2 or $TiO_{2−x}F_x$. The various peaks on the spectra represent various moieties

expected to exist. For example, the Ti atoms bonded to 3 F atoms at around 460.4 eV, described as a TiF_3 impurity.[31] Similarly, the Ti $2p_{1/2}$ component structures including three $Ti_3C_2T_x$ peaks (TiC, Ti^{2+}, and Ti^{3+}), and $TiO_2/TiO_{2−x}F_{2x}$ and TiF_3 were positioned at 461.2, 462.5, 463.7, 464.8, and 466 eV. A certain level of TiO_2 formation was observed for both the supernatant and the sediment of MXene after the washing process. By correlation between the area of peaks in the Ti 2p component, the percentages of $Ti_3C_2T_x$ and $TiO_2/TiO_{2−x}F_{2x}$ were determined to be approximately 73.87 and 57.78% and 18.28 and −35.74% for the sediment and the supernatant,

respectively (see Supporting Information Table S1). It revealed that the sediment sample was mainly composed of $Ti_3C_2T_x$ components, while the supernatant $Ti_3C_2T_x$ was largely oxidized into $TiO_2/TiO_{2-x}F_{2x}$. Therefore, the sediment of MXene is chosen for further surface patterning. The spectra for C 1s, O 1s, and F 1s, together with their peak fits, are presented in the Supporting Information (see Figure S1).

To demonstrate selective adsorption of MXene on a solid support, the surface is functionalized by μCP with monolayers that provide specific interactions with MXene surface moieties. The bare silicon wafer is used as a starting substrate and hydrolyzed by piranha solution to form a uniform oxide layer. It was followed by the monolayer formation of 3-amino-propyltriethoxysilane (APTES SAM), which was transferred by μCP in a 50 μm dot pattern. 1H,1H,2H,2H-Perfluorodecyl-triethoxysilane (POTS) molecules were introduced via vapor deposition to react with the remaining hydroxyl groups outside the dot pattern area to form a fluorinated monolayer (POTS SAM). Glutaraldehyde (GA) was used to activate the amino functional group of the APTES monolayer. Finally, the silicon wafer was immersed in an MXene-containing solution. The specific schematic of the micropatterned MXene procedure is illustrated in Figure 2.

All monolayer formations were first characterized by XPS (Figure 3) and water contact angle measurement (see Supporting Information Figures S2 and S3). The peak fitting of C 1s, N 1s, and O 1s spectral scanning allowed determination of different chemical bonds, which confirmed the surface functionalization's success. The monolayer formation process is illustrated in Figure 3A. APTES was printed onto a piranha-treated silicon by a flat PDMS stamp followed by immersion in GA solution. Figure 3B−D shows the XPS C 1s fitting results after each modification step. Printing APTES yielded an XPS peak at 285.8 eV (Figure 3C), assigned to the amino carbon chemical bond (N═C).[32] After immersion with GA solution, a carbonyl carbon peak (H−C═O) of aldehyde was determined at 288.2 eV (Figure 3D), which confirmed the GA SAM formation.[33] The appearance of N 1s after APTES modification indicated amino monolayer formation, exhibiting two peaks at 400.1 eV for amino groups bonded to carbon (C−NH$_2$) and at 401.8 eV assigned to a protonated amino (C−NH$_3^+$). Upon GA SAM formation, the main peak slightly shifted to a lower binding energy as imine bond formation (C−N═C) at 399.5 eV between amino groups of APTES and aldehyde groups of GA.[34] In addition, amine and protonated amine groups remained at 400.3 and 401.8 eV, which represent the unreacted amino group of APTES SAM (Figure 3G). The peak fitting of O 1s is relatively ambiguous to give any direct evidence for each monolayer modification. However, it can be mainly fitted as three peaks at 532.4, 532.8, and 531.7 eV, attributed to Si−OH, Si−O−Si, and H−C═O (Figure 3H−J).[35] The XPS results showed a successful functionalization of silicon with chemical bonding information between APTES and GA molecules and between molecules and surface silicon.

Following successful preparation of each monolayer, as in Figure 2, the silicon wafers with active functional surfaces were immersed with the MXene solution for 24 h. The MXene solution is prepared by dissolving the sediment of as-synthesized MXene in deionized water and delaminating via sonication for 5 min. Silicon samples after MXene solution immersion were rinsed with deionized water, sonicated for 5 min, and dried with nitrogen for further characterization.

Copious washing processes were carried out between each process step.

The SEM image clearly shows regular microscale dot patterns with a 50 μm diameter, consistent with the PDMS stamp feature (Figure 4A). The corresponding EDX mapping
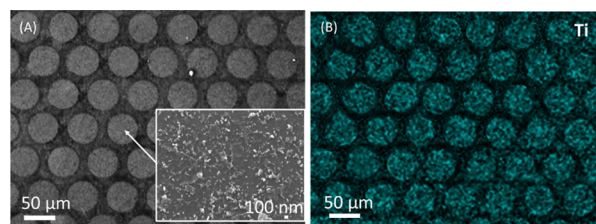

Figure 4. (A) SEM image of a substrate patterned with APTES SAM by μCP followed by GA SAM and with the outside surface passivated with POTS SAM. Afterward, the silicon substrate was incubated with delaminated MXene solution. Regular dots with a 50 μm diameter were observed. The inset image shows a higher magnification by FESEM where dot patterns contain a large and thin MXene layer. Small scattered MXene flakes also appeared. (B) Corresponding EDX mapping image of the Ti signal consistent with dot patterning.

image identifies the Ti signal shown as dot patterns, which provides chemical evidence for MXene adsorption (Figure 4B). This supports that MXene can be driven onto predefined patterns. In addition, amino functional groups of APTES SAM were activated by glutaraldehyde, further binding with −OH groups on the MXene surface. This covalent binding between MXene and the surface monolayer provides the stable formation of MXene patterns against the rinsing and sonication processes with consistent coverage in the defined region. A higher magnification in Figure 4A reveals the dot pattern composed of a thin MXene layer with scattered small MXene flakes. This small flake is due to the delamination step in the sonication bath during the MXene delamination process. Proper sonication power control should further improve the MXene delamination process by avoiding small flake generation.

Molecularly driven MXene assembly was carried out in an acid environment with HCl as a catalyst and the excess of MXene flakes. The oxygen terminations (−O groups) were converted to hydroxyl (−OH groups) in ambient acid.[36] The hemiacetal bonds were formed by a reaction between −OH groups on the MXene surface and aldehyde groups (H−C═O groups) of GA. However, in the presence of an acid and a large OH group of MXene, reversible hemiacetal bonds can undergo a transition reaction to form acetal bonds (Figure 5A), which are very strong and stable even in acidic and basic environments.[37]

The XPS results of the chemically assembled MXene layer with regions of Ti 2p, O 1s, C 1s, and F 1s are presented in Figure 5B−E. Upon the Ti 2p spectrum, component peaks of the assembled MXene layer are completely identical with the sediment $Ti_3C_2T_x$ used to prepare MXene solution (Figure 1C). MXene components, including Ti−C, Ti^{2+}, and Ti^{3+}, were defined with a dominant intensity of approximately 74.37% of the peak area ratio (Figure 5B). There were three peaks in the O 1s spectra belonging to MXene, located at 530, 531.7, and 532.3 eV, and labeled as C−Ti−O$_i$, C−Ti−O$_{ii}$, and C−Ti−OH, respectively (Figure 5C). These peaks are situated at the same location as O 1s of the as-synthesized MXene. However, significant changes of relative peak intensities were
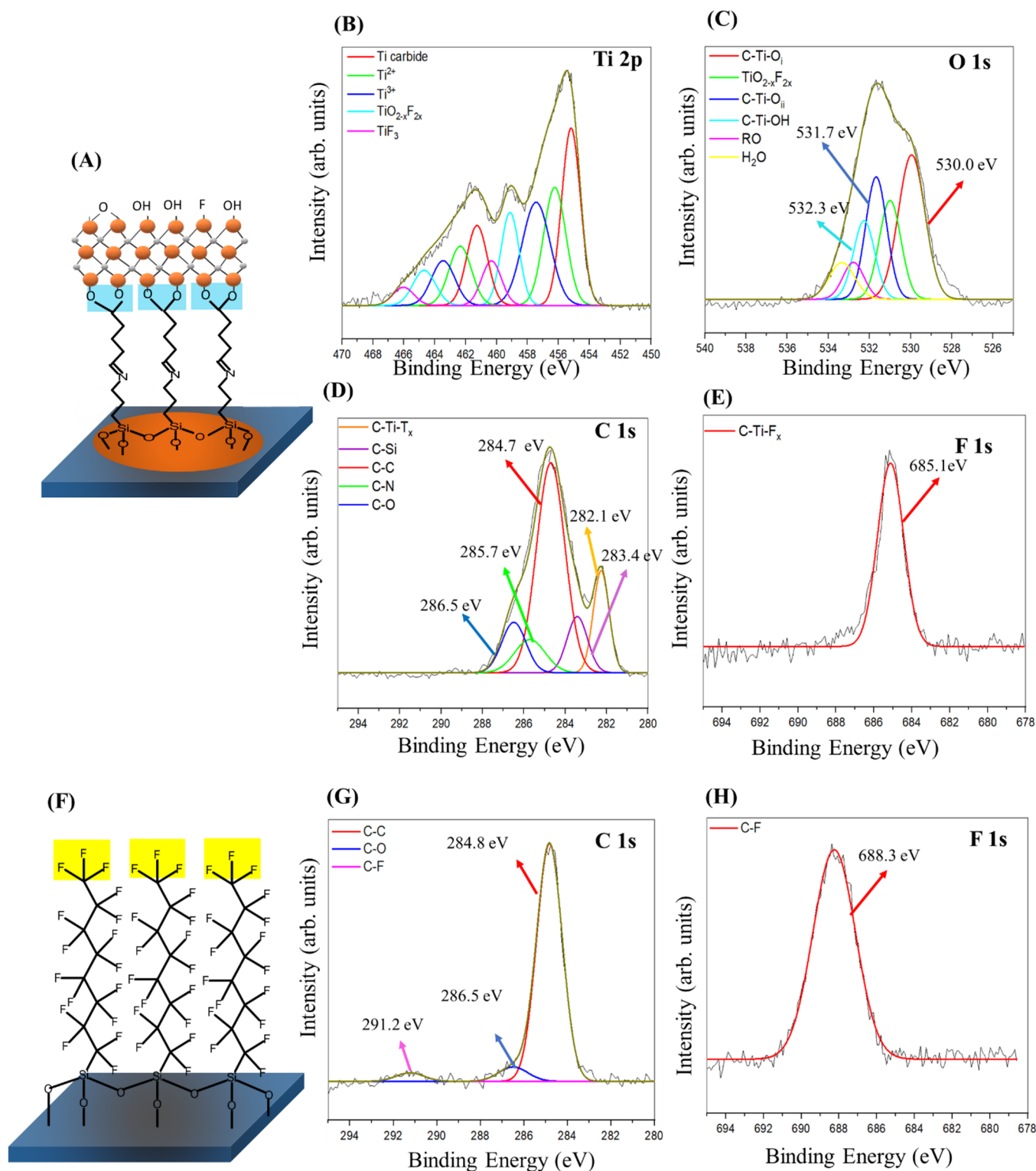
Figure 5. Schematic of the chemical structure of (A) assembled MXene layer via acetal bond formation (highlighted in blue) and (F) POTS SAM to improve selectivity via fluorinated moieties (highlighted in yellow). (B−E) XPS fitting results of Ti 2p, O 1s, C 1s, and F 1s of the assembled MXene layer formation showing covalent bonding with the active silicon surface. (G,H) C 1s and F 1s fitting results of POTS SAM formation. RO: organic component.

observed as indications of new bonding formation on the MXene. The increase in C−Ti−O$_i$ peak ratios in the MXene layer can be attributed to acetal bond formation, with similar binding energy at 530 eV. MXene with rich OH groups can react with aldehyde groups via covalent acetal bond formation

under acidic conditions. Moreover, the decrease in the C−Ti−OH peak ratio also indicated that hydroxyl groups on the MXene surface were converted to acetal bonds. The C 1s region was fitted into five peaks located at 282.1, 283.4, 284.7, 285.7, and 286.5 eV (Figure 5D). The position at 282.1 eV was
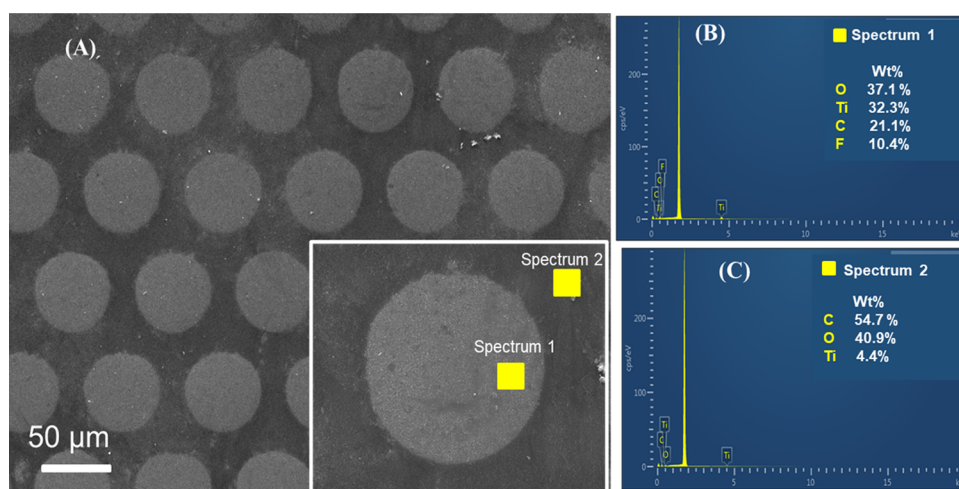
Figure 6. (A) SEM image of a substrate patterned with APTES SAM by μCP followed by GA SAM formation. The silicon substrate was incubated with MXene solution directly without POTS SAM passivation. (B,C) EDX scanning images showing a certain level of Ti signal (MXene) adsorption inside and outside dot patterns.

an identical representation of the as-synthesized MXene (see Supporting Information Figure S1). However, compared to the C 1s spectra of GA SAM (Figure 3D), a peak at 288.2 eV that represents H−C═O disappeared. This indicated that all aldehyde groups reacted entirely with OH groups on the MXene surface (Figure 5D). In addition, the F 1s spectrum remained identical to that of the as-synthesized MXene showing one peak at 685.1 eV attributed to MXene surface moieties (Figure 5E). Based on XPS fitting, it confirms the formation of proposed acetal bonding between MXene and GA SAM. In addition, the presence of the remaining C−Ti−OH on the MXene surface holds promise for further molecule attachment as a sensing application.

These results indicated that glutaraldehyde is an efficient cross-linking material that significantly improves MXene layer stability onto a silicon substrate. A control experiment was designed to reveal the MXene adsorption process without GA SAM. APTES SAM was incubated directly in MXene solution followed by the same rinsing procedure. The SEM image showed low coverage of MXene patterns compared to the pattern obtained with GA SAM. This can be understood as MXene adsorption onto APTES SAM via weak electrostatic interaction between −NH_3^+ and −OH^-. Therefore, the MXene pattern showed weak stability against rinsing and sonication (see Supporting Information Figure S4).

To improve the selectivity of MXene adsorption, POTS SAM was used as a passivation layer outside the patterning area to prevent unwanted reactions with glutaraldehyde (Figure 5F). Moreover, the hydrophobic nature of POTS SAM also dislikes the hydrophilic property of MXene given by −OH moieties. All these interactions will further prevent unnecessary adsorption of MXene outside APTES SAM patterned areas. 1H,1H,2H,2H-Perfluorooctyltriethoxysilane was assembled onto a silicon substrate by chemical vapor deposition, and XPS spectra in Figure 5G,H confirm POTS SAM formation.[38] The C 1s spectrum was attributed to three components, C−C, C−O, and C−F, located at 284.8, 286.5, and 291.2 eV, respectively. Upon the F 1s spectrum, only one component C−F peak at 688.3 eV was defined. The presence of the F element in both C 1s and F 1s proved the successful POTS SAM formation. A control experiment was carried out to demonstrate that POTS SAM was necessary for the

selectivity of MXene adsorption. A similar procedure was performed as previously but only no POTS SAM formation after APTES SAM. A silicon wafer was incubated with MXene solution after GA SAM. The SEM image and the EDS spectrum (Figure 6) show a certain level of MXene adsorption outside patterning areas. Therefore, hydrophobic fluorosilane as POTS SAM is suggested to enhance the selectivity of MXene adsorption.

The direct transfer of MXene was also studied by μCP onto a silicon substrate to evaluate patterning quality compared with molecularly driven adsorption. PDMS stamps with deeper features (17.6 μm) were fabricated from an etched Si mold, and MXene solution (25 mg/mL) in deionized water was obtained after sonication for 5 min. First, PDMS stamps were treated with oxygen plasma and stored in water before use. Next, the stamp was inked with MXene for 5 min and dried with nitrogen. Finally, the stamp was brought into contact with piranha-treated silicon with a controlled force for 5 min. Figure 7 presents dot patterns with a 100 μm diameter indicating the transfer of MXene. Printing with a 35 g weight shows better MXene coverage compared to printing without a weight. Therefore, pattern quality was significantly influenced by process control. For direct transfer printing, process
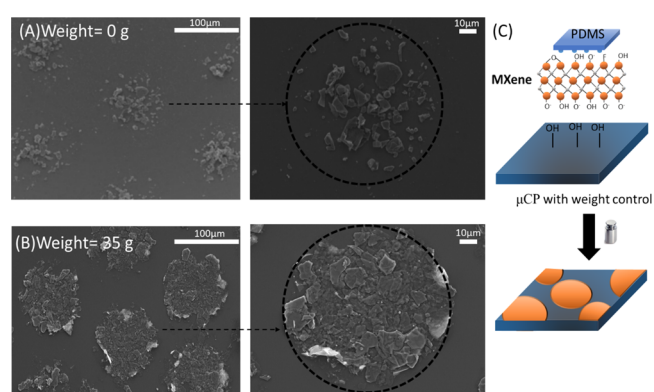

Figure 7. SEM images of a silicon substrate showing patterns of MXene by direct microcontact printing. Two different weights of (A) 0 and (B) 35 g were used to study the quality of MXene transfer. (C) Schematic of direct MXene patterning by μCP.
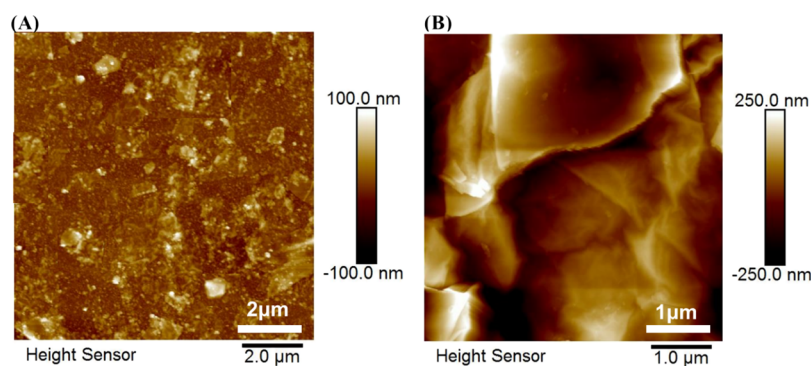
Figure 8. AFM images of (A) molecularly driven assembled MXene patterning and (B) direct MXene patterning by μCP.
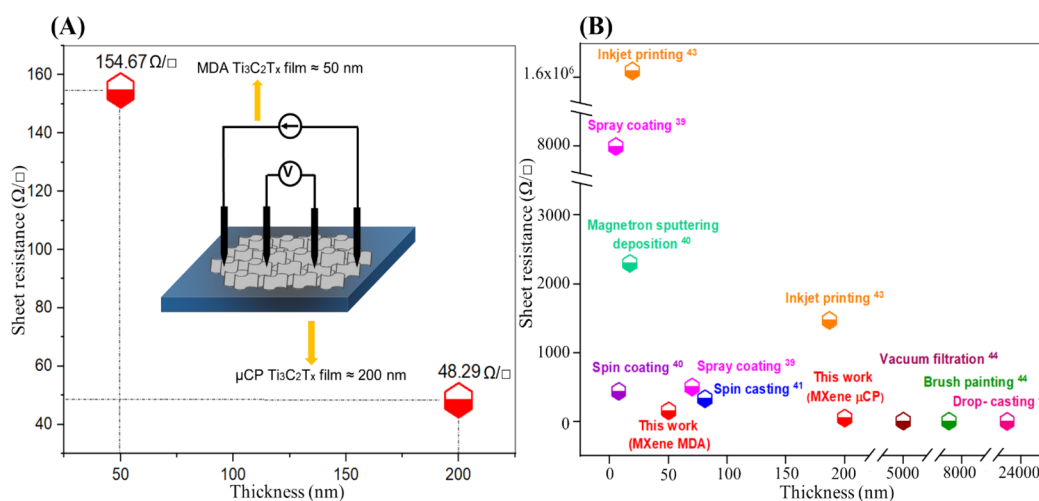

Figure 9. (A) Sheet resistance of MDA MXene and μCP MXene films by the four-point probe measurement. (B) Comparison of the specific sheet resistance corresponding to the thickness of MXene layers prepared by different techniques.

optimization is required to obtain consistent performance, such as solvent selection, stamp wettability, the level of solution drying, and the printing force. Moreover, varied sizes of MXene flakes with thicker layers were observed by direct microcontact printing, while the molecularly driven assembly obtained much smaller and thinner MXene flakes.

The molecularly driven assembled MXene layer was measured to have an approximately 50 nm thickness and an around 7.97 nm roughness by AFM (Figure 8A). The MXene layer by direct μCP is at least four times thicker than the assembled one and has a larger roughness of up to 77.8 nm. The thickness of the MXene layer by direct μCP was more than 200 nm, and some areas were even thicker than 1 μm. The smaller roughness and thickness of the molecularly driven assembled MXene film indicated its smooth and continuous surface, which will be much more effective in its electrical properties. At the same time, the thicker structure of direct μCP is due to the multilayer stacking of MXene flakes (Figure 7B). Moreover, the flake size of the molecularly driven assembled MXene layer is less than 1 μm, whose dimensions are shown in SEM images. The flakes transferred directly by μCP were observed with large sizes of 10 μm in diameter (see Supporting Information Figure S5).

The average sheet resistance values of the molecularly driven assembled MXene film (MDA MXene film) and the μCP MXene film are measured to be 154.67 (50 nm thickness) and 48.29 $\Omega/\square$ (200 nm thickness), respectively, by a four-point probe technique (Figure 9A). The four times lower resistance

of μCP MXene films than that of the MDA MXene film is due to the stacking of $Ti_3C_2T_x$ flakes, which is shown by the higher thickness of the MXene network. It is proper that the higher the thickness, the lower the sheet resistance of MXene films.[39−45] As mentioned above, a thicker layer of the sensing material is unfavorable to absorb target analytes of the MXene surface, so it is essential to obtain a thin material layer with low resistivity. Moreover, the thickness and sheet resistance are compared with various transferring techniques (Figure 9B). Among thin films with a thickness of around 5−250 nm, the current proposed molecularly driven assembled patterning technique showed an impressively lower resistance than other patterns prepared by different techniques. In detail, the sheet resistance of the MDA MXene film (154.67 $\Omega/\square$) is almost 10^4 times lower than that of inkjet printing[43] (1.66×10^6 $\Omega/\square$). Similarly, it is also lower from 3 to 52 times than the sheet resistance of spray coating[39] (500−8000 $\Omega/\square$) and 15 times lower than that of magnetron sputtering deposition (2300 $\Omega/\square$)[42] published previously. Furthermore, the sheet resistance of the chemically driven MXene film in this work is about twice and three times lower than those of spin coating/casting films (330[40] and 437 $\Omega/\square$[41]). Understandably, the nicely low sheet resistance of the MAD MXene film could result from the even surface (roughness $\approx$ 8 nm) and high coverage of the MXene layer. By contrast, the films obtained from brush painting ($\approx$ 4.98 $\Omega/\square$),[44] vacuum filtration (1−5 $\Omega/\square$),[44] and drop-casting ($\approx$1 $\Omega/\square$)[45] were estimated to have approximately 30−150 times lower sheet resistance than this MDA MXene

film but with much thicker MXene layers (detailed values are listed in Supporting Information Table S2). Compared to other transferring processes, the good conductivity of the MDA MXene film is the most suitable choice for MXene patterning as the sensing material with its low sheet resistance, thin film, area control, and stability over the substrate that is applicable for further sensing application.

4. CONCLUSIONS

The MXene field is still in its early stage of development. Researchers are working on exploring its applications in energy storage, electronics, optoelectronics, and sensing devices. Indeed, to realize its practical utilization, especially to facilitate commercialization potential, MXene immobilization onto a target support is essential to obtain a few layers of structures thinner than 100 nm simultaneously. This study demonstrates a new strategy using molecular interactions to drive MXene adsorption. Remarkable selectivity and surface coverage are obtained. In addition, the obtained MXene layer is with a thickness of around 50 nm and a sheet resistance of approximately 154.67 $\Omega/\square$, which are much lower than some other transferring techniques. This straightforward surface patterning technique will allow further applications, especially as sensing devices with reduced noise detection during the sensing process.

Moreover, MXene flakes obtained from the molecularly driven process are relatively smaller than those from direct transfer printing. This size selection is achieved naturally by the chemical bonding strength between MXene surface moieties and chemical functionalization on the target. This is beneficial if certain flake sizes are desired for different applications. One only needs to have a suitable master as the desired pattern by standard semiconductor lithography. Furthermore, this master can be repeatedly used to prepare PDMS stamps, and chemical patterns can be obtained accordingly. Eventually, MXene flakes will be driven and attached selectively onto those desired chemical patterns. Furthermore, this process did not alter the MXene pristine surface property since no other material (such as polymers) is introduced onto the MXene surface during the MXene solution preparation. Therefore, the exposed side of MXene patterns remains available for molecule binding as interactive sites, which allows adsorption of different gas or ion molecules. This can serve as a simple method for MXene-based sensing device scaling or applications that require conformal modification of MXene flakes, especially with dimensional structures.

ASSOCIATED CONTENT

Supporting Information

The Supporting Information is available free of charge at https://pubs.acs.org/doi/10.1021/acsomega.1c06662.

> Detailed XPS and water contact angle characterization of MXene, APTES SAM, GA SAM, and POTS SAM; control experiment of MXene assembly with APTES SAM (PDF)

AUTHOR INFORMATION

Corresponding Authors

Chao-An Jong − National Applied Research Laboratories, Taiwan Semiconductor Research Institute, Hsinchu 300091, Taiwan; Email: cajong@narlabs.org.tw

Shu-Han Hsu − Sirindhorn International Institute of Technology, Thammasat University, Khlong Nueng, Pathum Thani 12120, Thailand; orcid.org/0000-0001-6055-9330; Email: shuhanhsu@siit.tu.ac.th

Shih-Feng Tseng − Department of Mechanical Engineering, National Taipei University of Technology, Taipei 106344, Taiwan; Email: tsf@ntut.edu.tw

Author

Linh Chi T. Cao − Sirindhorn International Institute of Technology, Thammasat University, Khlong Nueng, Pathum Thani 12120, Thailand

Complete contact information is available at:
https://pubs.acs.org/10.1021/acsomega.1c06662

Notes

The authors declare no competing financial interest.

REFERENCES

(1) Anasori, B.; Lukatskaya, M. R.; Gogotsi, Y. 2D Metal Carbides and Nitrides (MXenes) for Energy Storage. *Nat. Rev. Mater.* 2017, DOI: 10.1038/natrevmats.2016.98.

(2) Pang, J.; Mendes, R. G.; Bachmatiuk, A.; Zhao, L.; Ta, H. Q.; Gemming, T.; Liu, H.; Liu, Z.; Rummeli, M. H. Applications of 2D MXenes in Energy Conversion and Storage Systems. *Chem. Soc. Rev.* 2019, 48, 72−133.

(3) Wu, X.; Han, B.; Zhang, H.-B.; Xie, X.; Tu, T.; Zhang, Y.; Dai, Y.; Yang, R.; Yu, Z.-Z. Compressible, Durable and Conductive Polydimethylsiloxane-Coated MXene Foams for High-Performance Electromagnetic Interference Shielding. *Chem. Eng. J.* 2020, 381, 122622.

(4) Ling, Z.; Ren, C. E.; Zhao, M. Q.; Yang, J.; Giammarco, J. M.; Qiu, J.; Barsoum, M. W.; Gogotsi, Y. Flexible and Conductive MXene Films and Nanocomposites with High Capacitance. *Proc. Natl. Acad. Sci. U. S. A.* 2014, 16676.

(5) Zhan, X.; Si, C.; Zhou, J.; Sun, Z. MXene and MXene-Based Composites: Synthesis, Properties and Environment-Related Applications. *Nanoscale Horizons* 2020, 5, 235−258.

(6) Wei, Z.; Peigen, Z.; Wubian, T.; Xia, Q.; Yamei, Z.; ZhengMing, S. Alkali Treated Ti3C2Tx MXenes and Their Dye Adsorption Performance. *Mater. Chem. Phys.* 2018, 206, 270−276.

(7) Satheeshkumar, E.; Makaryan, T.; Melikyan, A.; Minassian, H.; Gogotsi, Y.; Yoshimura, M. One-Step Solution Processing of Ag, Au and Pd@MXene Hybrids for SERS. *Sci. Rep.* 2016, 6, 32049.

(8) Sinha, A.; Dhanjai; Zhao, H.; Huang, Y.; Lu, X.; Chen, J.; Jain, R. MXene: An Emerging Material for Sensing and Biosensing. *TrAC, Trends Anal. Chem.* 2018, 105, 424−435.

(9) Khazaei, M.; Mishra, A.; Venkataramanan, N. S.; Singh, A. K.; Yunoki, S. Recent Advances in MXenes: From Fundamentals to Applications. *Curr. Opin. Solid State Mater. Sci.* 2019, 23, 164−178.

(10) An, H.; Habib, T.; Shah, S.; Gao, H.; Radovic, M.; Green, M. J.; Lutkenhaus, J. L. Surface-Agnostic Highly Stretchable and Bendable Conductive MXene Multilayers. *Sci. Adv.* 2018, 4, 1−9.

(11) Guo, Y.; Zhong, M.; Fang, Z.; Wan, P.; Yu, G. A Wearable Transient Pressure Sensor Made with MXene Nanosheets for Sensitive Broad-Range Human-Machine Interfacing. *Nano Lett.* 2019, 19, 1143−1150.

(12) Zhu, X.; Liu, B.; Hou, H.; Huang, Z.; Zeinu, K. M.; Huang, L.; Yuan, X.; Guo, D.; Hu, J.; Yang, J. Alkaline Intercalation of Ti3C2 MXene for Simultaneous Electrochemical Detection of Cd(II),

Pb(II), Cu(II) and Hg(II); Elsevier Ltd, 2017; Vol. 248, DOI: 10.1016/j.electacta.2017.07.084.

(13) Desai, M. L.; Basu, H.; Singhal, R. K.; Saha, S.; Kailasa, S. K. Ultra-Small Two Dimensional MXene Nanosheets for Selective and Sensitive Fluorescence Detection of Ag + and Mn 2+ Ions. *Colloids Surf., A* **2019**, *565*, 70−77.

(14) Xu, B.; Zhu, M.; Zhang, W.; Zhen, X.; Pei, Z.; Xue, Q.; Zhi, C.; Shi, P. Ultrathin MXene-Micropattern-Based Field-Effect Transistor for Probing Neural Activity. *Adv. Mater.* **2016**, 3333.

(15) Kim, S. J.; Koh, H.-J.; Ren, C. E.; Kwon, O.; Maleski, K.; Cho, S.-Y.; Anasori, B.; Kim, C.-K.; Choi, Y.-K.; Kim, J.; Gogotsi, Y.; Jung, H.-T. Metallic Ti$_3$C$_2$T$_x$ MXene Gas Sensors with Ultrahigh Signal-to-Noise Ratio. *ACS Nano* **2018**, *12*, 986−993.

(16) Zhang, Y. Z.; Wang, Y.; Jiang, Q.; El-Demellawi, J. K.; Kim, H.; Alshareef, H. N. MXene Printing and Patterned Coating for Device Applications. *Adv. Mater.* **2020**, *32*, 1908486.

(17) Kim, H.; Alshareef, H. N. MXetronics: MXene-Enabled Electronic and Photonic Devices. *ACS Mater. Lett.* **2020**, *2*, 55−70.

(18) Hart, J. L.; Hantanasirisakul, K.; Lang, A. C.; Anasori, B.; Pinto, D.; Pivak, Y.; van Omme, J. T.; May, S. J.; Gogotsi, Y.; Taheri, M. L. Control of MXenes' Electronic Properties through Termination and Intercalation. *Nat. Commun.* **2019**, *10*, 552.

(19) Dong, L.; Kumar, H.; Anasori, B.; Gogotsi, Y.; Shenoy, V. B. Rational Design of Two-Dimensional Metallic and Semiconducting Spintronic Materials Based on Ordered Double-Transition-Metal MXenes. *J. Phys. Chem. Lett.* **2017**, *8*, 422−428.

(20) Jiang, X.; Kuklin, A. V.; Baev, A.; Ge, Y.; Ågren, H.; Zhang, H.; Prasad, P. N. Two-Dimensional MXenes: From Morphological to Optical, Electric, and Magnetic Properties and Applications. *Phys. Rep.* **2020**, *848*, 1−58.

(21) Perl, A.; Reinhoudt, D. N.; Huskens, J. Microcontact Printing: Limitations and Achievements. *Adv. Mater.* **2009**, *21*, 2257−2268.

(22) Hsu, S.-H.; Reinhoudt, D. N.; Huskens, J.; Velders, A. H. Imidazolide Monolayers for Reactive Microcontact Printing. *J. Mater. Chem.* **2008**, *18*, 4959−4963.

(23) González-Campo, A.; Hsu, S. H.; Puig, L.; Huskens, J.; Reinhoudt, D. N.; Velders, A. H. Orthogonal Covalent and Noncovalent Functionalization of Cyclodextrin-Alkyne Patterned Surfaces. *J. Am. Chem. Soc.* **2010**, *132*, 11434−11436.

(24) Lamping, S.; Ravoo, B. J. Hybrid TiO2/Metal Nanoparticle Microstructures Made by Microcontact Printing, Absorption and Electroless Deposition. *J. Mater. Chem. C* **2017**, *5*, 5882−5886.

(25) Molina-Lopez, F.; Briand, D.; De Rooij, N. F. Inkjet and Microcontact Printing of Functional Materials on Foil for the Fabrication of Pixel-like Capacitive Vapor Microsensors. *Org. Electron.* **2015**, *16*, 139−147.

(26) Jain, A.; Bharadwaj, P.; Heeg, S.; Parzefall, M.; Taniguchi, T.; Watanabe, K.; Novotny, L. Minimizing Residues and Strain in 2D Materials Transferred from PDMS. *Nanotechnology* **2018**, *29*, 265203.

(27) Ogihara, H.; Kibayashi, H.; Saji, T. Microcontact Printing for Patterning Carbon Nanotube/Polymer Composite Films with Electrical Conductivity. *ACS Appl. Mater. Interfaces* **2012**, *4*, 4891−4897.

(28) Xiao, P.; Gu, J.; Chen, J.; Zhang, J.; Xing, R.; Han, Y.; Fu, J.; Wang, W.; Chen, T. Micro-Contact Printing of Graphene Oxide Nanosheets for Fabricating Patterned Polymer Brushes. *Chem. Commun.* **2014**, *50*, 7103−7106.

(29) Alhabeb, M.; Maleski, K.; Anasori, B.; Lelyukh, P.; Clark, L.; Sin, S.; Gogotsi, Y. Guidelines for Synthesis and Processing of Two-Dimensional Titanium Carbide (Ti$_3$C$_2$T$_x$ MXene). *Chem. Mater.* **2017**, *29*, 7633−7644.

(30) Halim, J.; Cook, K. M.; Naguib, M.; Eklund, P.; Gogotsi, Y.; Rosen, J.; Barsoum, M. W. X-Ray Photoelectron Spectroscopy of Select Multi-Layered Transition Metal Carbides (MXenes). *Appl. Surf. Sci.* **2016**, 406.

(31) Benchakar, M.; Loupias, L.; Garnero, C.; Bilyk, T.; Morais, C.; Canaff, C.; Guignard, N.; Morisset, S.; Pazniak, H.; Hurand, S.; Chartier, P.; Pacaud, J.; Mauchamp, V.; Barsoum, M. W.; Habrioux, A.; Célérier, S. One MAX Phase, Different MXenes: A Guideline to

Understand the Crucial Role of Etching Conditions on Ti3C2Tx Surface Chemistry. *Appl. Surf. Sci.* **2020**, *530*, 147209.

(32) Hijazi, M.; Stambouli, V.; Rieu, M.; Barnier, V.; Tournier, G.; Demes, T.; Viricelle, J.-P.; Pijolat, C. Synthesis and Characterization of Tin Dioxide Thick Film Modified by APTES in Vapor and Liquid Phases. *J. Mater. Sci.* **2018**, *53*, 727−738.

(33) Al-Ani, A.; Pingle, H.; Reynolds, N. P.; Wang, P.-Y.; Kingshott, P. Tuning the Density of Poly(Ethylene Glycol) Chains to Control Mammalian Cell and Bacterial Attachment. *Polymers (Basel).* **2017**, *9*, 343.

(34) Kehrer, M.; Duchoslav, J.; Hinterreiter, A.; Cobet, M.; Mehic, A.; Stehrer, T.; Stifter, D. XPS Investigation on the Reactivity of Surface Imine Groups with TFAA. *Plasma Processes Polym.* **2019**, *16*, 1800160.

(35) Lee, S. W.; Gallant, B. M.; Lee, Y.; Yoshida, N.; Kim, D. Y.; Yamada, Y.; Noda, S.; Yamada, A.; Yang, S.-H. Self-Standing Positive Electrodes of Oxidized Few-Walled Carbon Nanotubes for Light-Weight and High-Power Lithium Batteries. *Energy Environ. Sci.* **2012**, *5*, 5437−5444.

(36) Ibragimova, R.; Puska, M. J.; Komsa, H.-P. PH-Dependent Distribution of Functional Groups on Titanium-Based MXenes. *ACS Nano* **2019**, *13*, 9171−9181.

(37) Saunders, W. H. Physical Organic Chemistry. Second Edition. *J. Am. Chem. Soc.* **1963**, *85*, 1366−1367.

(38) Srinivasan, U.; Houston, M. R.; Howe, R. T.; Maboudian, R. Alkyltrichlorosilane-Based Self-Assembled Monolayer Films for Stiction Reduction in Silicon Micromachines. *J. Microelectromech. Syst.* **1998**, *7*, 252−260.

(39) Hantanasirisakul, K.; Zhao, M.-Q.; Urbankowski, P.; Halim, J.; Anasori, B.; Kota, S.; Ren, C. E.; Barsoum, M. W.; Gogotsi, Y. Fabrication of Ti$_3$C$_2$T$_x$ MXene Transparent Thin Films with Tunable Optoelectronic Properties. *Adv. Electron. Mater.* **2016**, *2*, 1−7.

(40) Halim, J.; Lukatskaya, M. R.; Cook, K. M.; Lu, J.; Smith, C. R.; Näslund, L. Å.; May, S. J.; Hultman, L.; Gogotsi, Y.; Eklund, P.; Barsoum, M. W. Transparent Conductive Two-Dimensional Titanium Carbide Epitaxial Thin Films. *Chem. Mater.* **2014**, *26*, 2374−2381.

(41) Dillon, A. D.; Ghidiu, M. J.; Krick, A. L.; Griggs, J.; May, S. J.; Gogotsi, Y.; Barsoum, M. W.; Fafarman, A. T. Highly Conductive Optical Quality Solution-Processed Films of 2D Titanium Carbide. *Adv. Funct. Mater.* **2016**, *26*, 4162−4168.

(42) Mariano, M.; Mashtalir, O.; Antonio, F. Q.; Ryu, W. H.; Deng, B.; Xia, F.; Gogotsi, Y.; Taylor, A. D. Solution-Processed Titanium Carbide MXene Films Examined as Highly Transparent Conductors. *Nanoscale* **2016**, *8*, 16371−16378.

(43) Wen, D.; Wang, X.; Liu, L.; Hu, C.; Sun, C.; Wu, Y.; Zhao, Y.; Zhang, J.; Liu, X.; Ying, G. Inkjet Printing Transparent and Conductive MXene (Ti3C2Tx) Films: A Strategy for Flexible Energy Storage Devices. *ACS Appl. Mater. Interfaces* **2021**, *13*, 17766−17780.

(44) Seok, S.-H.; Choo, S.; Kwak, J.; Ju, H.; Han, J. H.; Kang, W.-S.; Lee, J.; Kim, S.-Y.; Lee, D. H.; Lee, J.; Wang, J.; Song, S.; Jo, W.; Jung, B. M.; Chae, H. G.; Son, J. S.; Kwon, S.-Y. Synthesis of High Quality 2D Carbide MXene Flakes Using a Highly Purified MAX Precursor for Ink Applications. *Nanoscale Adv.* **2021**, *3*, 517−527.

(45) Lipton, J.; Röhr, J. A.; Dang, V.; Goad, A.; Maleski, K.; Lavini, F.; Han, M.; Tsai, E. H. R.; Weng, G.-M.; Kong, J.; Riedo, E.; Gogotsi, Y.; Taylor, A. D. Scalable, Highly Conductive, and Micropatternable MXene Films for Enhanced Electromagnetic Interference Shielding. *Matter* **2020**, *3*, 546−557.